Formulation of Fast-Disintegrating Drug Delivery System from Cyclodextrin/Naproxen Inclusion Complex Nanofibrous Films

Journal:	*RSC Medicinal Chemistry*
Manuscript ID	MD-RES-10-2023-000557.R2
Article Type:	Research Article
Date Submitted by the Author:	09-Dec-2023
Complete List of Authors:	Celebioglu, Asli; Cornell University, Fiber Science Dash, Kareena; Cornell University Aboelkheir, Mahmoud; Cornell University, Fiber Science Program, Department of Human Centered Design Kilic, Mehmet; Korea Institute of Science and Technology, Computational Science Research Center; Durgun, Engin; Bilkent University Uyar, Tamer; Cornell University, Department of Fiber Science & Apparel Design

ARTICLE

Formulation of Fast-Disintegrating Drug Delivery System from Cyclodextrin/Naproxen Inclusion Complex Nanofibrous Films

Received 00th January 20xx,
Accepted 00th January 20xx

DOI: 10.1039/x0xx00000x

Asli Celebioglu[a], Kareena Dash[b], Mahmoud Aboelkheir[a], Mehmet E. Kilic[c], Engin Durgun[d] and Tamer Uyar[a]*

Naproxen is a well-known non-steroidal anti-inflammatory drug (NSAID) that suffers from limited water solubility. The inclusion complexation with cyclodextrin (CD) can eliminate this drawback and free-standing nanofibrous film (NF) generated from these inclusion complexes (IC) can be a promising alternative formula as an orally disintegrating drug delivery system. For this, naproxen/CD IC NM were generated using the highly water soluble hydroxypropylated derivate of βCD (HPβCD) with two different molar ratios of 1/1 and 1/2 (drug/CD). The complexation energy calculated by the modeling study demonstrated a more favorable interaction between HPβCD and naproxen for 1/2 molar ratio than 1/1. HPβCD/naproxen IC NM were generated with loading concentration of ~ 7-11 % and without using toxic chemicals. HPβCD/naproxen IC NM indicated a faster and enhanced release profile in aqueous medium compared to pure naproxen owing to inclusion complexation. Moreover, a rapid disintegration in less than a second was obtained in an artificial saliva environment.

Introduction

One of the major issues in the pharmaceutical industry is the rising number of poorly water-soluble drugs and their low bioavailability to the human body. Over 70% of new chemical entities in the drug discovery pipeline are nearly insoluble in water, leading to slow drug absorption, gastrointestinal toxicity, and insufficient bioavailability.[1,2] In response to this problem, fast-disintegrating oral drug delivery systems have gained increasing amounts of attention due to their ability to provide rapid and enhanced drug absorption, and improved bioavailability by reducing the hepatic first-pass effect.[3,4] Fast-disintegrating systems are generally in flexible, thin, and free-standing strip/film forms having hygroscopic profiles which enable the dissolving of these systems in a moist environment by eliminating the use of water. Here, the fast disintegration of the delivery system in the oral mucosa removes the choking hazard and need for swallowing which results in a rise in patient compliance.[3–5] Therefore, fast-disintegrating oral drug delivery systems are useful alternative pharmaceutical forms to tablets and capsules. Fast-disintegrating systems can be generated through processes such as freeze drying, granulation, molding, compression, spraying etc. which are meant to enhance the dissolution rate and so bioavailability of the drugs.[6] On the other hand, the technique of electrospinning has become a prominent approach for engineering nanomaterials in the form of free-standing fibrous films as carriers of chemical and biological compounds in therapeutic applications.[7–9] The unique properties of electrospun nanofibers such as highly porous structure, high surface area, lightweight and drug encapsulation capability makes these fibrous films attractive for the emerging orally fast-disintegrating delivery system.[10] Moreover, the potential of these nanofibrous films can verified by using different configurations of electrospinning such as coaxial[11], triaxial[12] and side-by-side.[13]

For developing water-soluble nanofibrous films with quick disintegration times, different types of natural and synthetic hydrophilic polymers have been employed including polyvinyl alcohol (PVA)[14,15], poly(ethylene oxide) (PEO)[15], polyvinylpyrrolidone (PVP)[15,16], pullulan[17,18], etc. just as used for commercially available orally disintegrating films (ODFs).[19] However, toxic solvents, additional chemicals or high processing temperature might be required for proper incorporation of drug molecules into the electrospun polymer matrices. At this point, cyclodextrin (CD) drug inclusion complexes electrospun into nanofibrous films without using a polymer or another toxic chemical can circumvent the problems present in polymer-based drug carrier systems.[20–27] CDs playing a key role in drug encapsulation, are a class of oligosaccharides derived from starch. CDs are non-toxic and bio-safe molecules having a donut shape which enables the formation of inclusion complexes with various hydrophobic compounds by

[a] Fiber Science Program, Department of Human Centered Design, College of Human Ecology, Cornell University, Ithaca, NY, 14853, USA
[b] Biological Sciences, College of Arts and Sciences, Cornell University, Ithaca, NY, 14853, USA
[c] Computational Science Research Center, Korea Institute of Science and Technology, Seoul, 02792, Republic of Korea
[d] UNAM-National Nanotechnology Research Center and Institute of Materials Science and Nanotechnology, Bilkent University, Ankara 06800, Turkey

*Corresponding Author: TU: tu46@cornell.edu

Electronic Supplementary Information (ESI) available: [details of any supplementary information available should be included here]. See DOI: 10.1039/x0xx00000x

encapsulating them into the relatively hydrophobic inner cavity of CDs. Here, the inclusion complexation can increase the water solubility, bioavailability, and stability of the encapsulated bioactive compounds and this ensures a widespread application for CDs and their inclusion complexes particularly across the medicine, pharmacy, and biotechnology areas.[10,28,29]

Naproxen is a non-steroidal anti-inflammatory drug (NSAID) that is used to reduce the inflammation, fever and pain during the treatment of migraine, arthritis, kidney stones, gout, menstrual cramps, etc. However, the poorly water-soluble nature of naproxen limits its usage for pharmaceutical administrations.[30] As it was reported previously, this shortcoming of naproxen can be dissolved by forming inclusion complexes with different types of CD molecules.[30–37] Even, in a related study by Séon-Lutz et al., hyaluronic acid/PVA nanofibers were incorporated with the inclusion complexes of hydroxypropyl-beta-cyclodextrin (HPβCD) and naproxen for the purpose of wound dressing applications.[38] In another study reported by Uyar Group, poly(ε-caprolactone) (PCL) nanofibers were functionalized with naproxen/βCD inclusion complexes that provided an enhanced release profile for drug molecule compared to CD-free system.[39] In this study, HPβCD was used to form inclusion complexes with naproxen and then for the electrospinning of this complex system in the absence of any polymer or organic solvents (Fig. 1). The potential and the favourableness of naproxen/HPβCD inclusion complex nanofibrous films as a fast-disintegrating delivery system were revealed using morphological, structural, and pharmacotechnical characterization techniques.

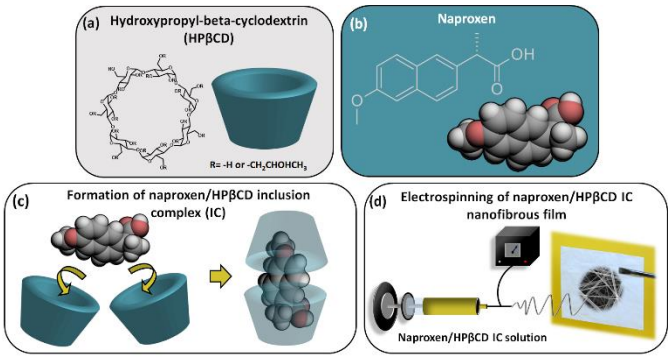

Fig. 1. Chemical structure of (a) hydroxypropyl-beta-cyclodextrin (HPβCD) and (b) naproxen. Schematic representation of (c) inclusion complex formation between naproxen and HPβCD molecules, and (d) electrospinning of naproxen/HPβCD IC nanofibrous film.

Experimental

Materials

Naproxen (99.3%, MP Biomedicals), buffer chemicals (phosphate buffered saline tablet (Sigma Aldrich), sodium phosphate dibasic heptahydrate (Na_2HPO_4, 98.0−102.0%, Fisher Chemical), sodium chloride (NaCl, >99%, Sigma-Aldrich), potassium phosphate monobasic (KH_2PO_4, ≥99.0%, Fisher Chemical), o-phosphoric acid (85%, Fisher Chemical), hydrochloric acid (Sigma-Aldrich, Ph. Eur., BP, NF, fuming, 36.5-38%)), dimethyl sulfoxide (DMSO, certified ACS, Fisher Chemical) and deuterated dimethyl sulfoxide (DMSO-*d6*, deuteration degree min. 99.8%, Cambridge Isotope) were obtained commercially. Hydroxypropyl-beta-cyclodextrin (HPβCD) (Cavasol® W7 HP, standard grade, molar substitution degree: ~0.9) was gifted from Wacker Chemie AG (USA). The Millipore Milli-Q ultrapure water system was used for distilled water.

Preparation of inclusion complex systems and electrospinning process

The clear solutions of HPβCD were prepared with CD concentration of 180 % (w/w, with respect to solvent) in distilled water (500 µL). Afterwards, naproxen was added to the clear HPβCD solutions to separately attain 1/1 and 1/2 molar ratios (drug/CD) that were corresponding to ~ 13.3 % (w/w, with respect to total sample amount) and ~ 7.1 % (w/w) of naproxen content in ultimate nanofibrous film. To form inclusion complexes (ICs), the naproxen/HPβCD solutions were stirred overnight at RT. Pure HPβCD solution (180 % (w/w)) was prepared as control sample. The conductivity and viscosity of all these aqueous systems were determined prior the electrospinning procedure. The conductivity of solutions was measured using conductivity-meter (FiveEasy, Mettler Toledo, USA) while viscosity was measured by a rheometer (AR 2000 rheometer, TA Instrument, USA, cone-plate spindle (20 mm, 4°), shear rate (0.01-1000 s^{-1}). The electrospinning solutions of naproxen/HPβCD ICs and pure HPβCD were individually transferred to 1 mL plastic syringe that fixed with 27 G needles. The electrospinning process was conducted in an electrospinning equipment (Spingenix, model: SG100, Palo Alto, USA). For this, the solution loaded syringes were placed on syringe pump and pushed with flow rate of 0.3 mL/h. The high voltage power source was set to 17.5 kV to apply voltage to the needle for the deposition of nanofibers on the fixed metal collector. During the process, the relative humidity and temperature were recorded at around 26 % and 20 °C, respectively.

Structural characterization

The morphology of naproxen/HPβCD (1/1) IC, naproxen/HPβCD (1/2) IC and HPβCD nanofibrous film was examined through scanning electron microscopy (SEM, Tescan MIRA3, Czech Republic). Prior the measurement, samples fixed on the SEM stub were coated with a layer of Au/Pd to eliminate the charging problem. The average diameter of fibers was defined following SEM imaging by using ImageJ software upon calculating ~100 fibers for each sample.

The inclusion complex formation within naproxen/HPβCD IC nanofibrous films were confirmed using different techniques. Firstly, attenuated total reflectance Fourier transform infrared spectroscopy (ATR-FTIR, PerkinElmer, USA) was used for this purpose. FTIR spectra of nanofibrous film and pure naproxen were recorded with 32 scans in the range of 4000-600 cm^{-1} and at a resolution of 4 cm^{-1}. X-ray diffractometer (XRD, Bruker D8 Advance ECO, Germany) also established the IC formation within nanofibrous films by analyzing the conversion of naproxen crystals into amorphous state by complexation. XRD measurements of nanofibrous film and naproxen were performed in the range of 2Θ=5º-30º using Cu-Kα radiation, 40 kV and 25 mA. The amorphization of naproxen was also confirmed using differential scanning calorimeter (DSC, TA Instruments Q2000, USA). The DSC thermograms were obtained by heating samples which were placed in T-zero Al pan from 0 °C to 200 °C using 10°C/min heating rate. On the other hand, thermal gravimetric

analyzer (TGA, TA Instruments Q500, USA) informed about the thermal degradation profile of samples which were located on the platinum pan and heated in the range of RT- 500°C in the increments of 20°C/min.

Loading efficiency

To calculate the loading efficiency of naproxen/HPβCD (1/1) IC and naproxen/HPβCD (1/2) IC nanofibrous films, ~ 1 mg of samples were dissolved in 5 mL of DMSO. Here, DMSO was selected to ensure the complete dissolution of components of naproxen and HPβCD within nanofibrous films. The naproxen content was measured using UV-vis spectroscopy (Perkin Elmer, Lambda 35, USA) (274 nm) and the calibration curve of naproxen in DMSO was obtained with $R^2 \geq 0.99$. The loading efficiency (%) was calculated by using the following formula;

$$\text{Loading efficiency (\%)} = Ce/Ct \times 100 \quad \text{(Formula 1)}$$

where Ce is the concentration of loaded naproxen and Ct the initial concentration of naproxen in the nanofibrous films. The measurements were repeated three times to attain an average ± standard deviation of results. Proton nuclear magnetic resonance spectroscopy (^{1}H-NMR) was also operated to analyze the chemical structure and to determine the loading efficiency of nanofibrous films roughly. For this, naproxen/HPβCD (1/1) IC, naproxen/HPβCD (1/2) IC nanofibrous films and naproxen were separately dissolved in *d6*-DMSO, and then placed in the ^{1}H-NMR spectrometer (Bruker AV500, with autosampler) for recording the ^{1}H-NMR spectra (16 scans). The results were examined by using Mestrenova software to calculate molar ratios through integrating characteristic peaks of components.

2D-NMR Measurement

The Rotating frame Overhauser Effect Spectroscopy (ROESY) method was applied to examine inclusion complex formation between HPβCD and naproxen. Here, 2D-NMR measurement was performed using 600 MHz Varian INOVA nuclear magnetic resonance spectrometer in D_2O at 25 °C.

Computational Methodology

To reveal the inclusion complex formation mechanisms at the atomic scale, ab initio quantum mechanical calculations based on density functional theory[40] were performed using VASP software.[41] The element potentials were described by the projector-augmented-wave method, and the size of the plane-wave basis set was determined by kinetic energy cut-off, which was fixed to 520 eV. The exchange-correlation potential was approximated by the Perdew-Burke-Ernzerhof (PBE) form of generalized gradient approximation (GGA), and van der Walls interactions were taken into account by Grimme's dispersion correction (DFT-D2) method.[42] The HPβCD, naproxen molecules, and their inclusion complexes were relaxed by the conjugate-gradient algorithm with precise energy (for self-consistent electronic steps) and force (for each ion) convergence criteria, which were 0.01 meV and 0.01 eV/Å, respectively. The solvent effect was included in calculations by the implicit solvation approach.[43]

Pharmacotechnical properties

The phase solubility profile of naproxen in the existence of CD was investigated by mixing the excess amount of naproxen (~ 6 mg) with increasing concentrations of HPβCD in the range of 0-32 mM in 5 mL of unbuffered water consequently showing pH in the range of 5.6-4.1. The mixtures were shaken on the orbital shaker (450 rpm) for 24 h at RT. Afterwards, the aqueous systems were filtered using disposable PTFE filter (0.45 µm) and UV-vis spectroscopy was used to record the absorbance intensity of aliquots at 230 nm. The calibration curve ($R^2 \geq 0.99$) of naproxen in water/ethanol (7/3, v/v) was applied to convert absorbance intensity into concentration (mM). For each system, the measurements were performed three times (average ± standard deviation). In addition, the binding constant (K_S) was calculated using the linear part of the phase solubility diagram by applying the following formula;

$$K_S = \text{slope}/S_0(1\text{-slope}) \quad \text{(Formula 2)}$$

where S_0 is the intrinsic solubility of naproxen (~0.4 mM).

The *in vitro* time-dependent release profiles of naproxen/HPβCD (1/1) IC and naproxen/HPβCD (1/2) IC nanofibrous films were analyzed in PBS buffer having pH 7.4. For this, ~ 10 mg of samples were immersed in 10 mL of buffer solution and shaken on an orbital shaker at 200 rpm and 37 °C. The aliquots of 100 µL were taken from each sample system at the particular time intervals (30 s to 10 min) and then 100 µL of fresh PBS buffer readded into the same systems. For each sample, tests were repeated three times (average ± standard deviation) and the absorbance intensity of removed aliquots was measured using UV-vis spectroscopy (230 nm). The calibration curve ($R^2 \geq 0.99$) of naproxen in PBS/ethanol (7/3, v/v) was applied to convert absorbance intensity into release concentration (ppm). As control, the release profile of pure naproxen (~ 1.3 mg) in the buffer system (pH 7.4, 10mL) was also examined using the drug concentration of ~ 0.6 mM which is higher than its intrinsic solubility (~ 0.4 mM) and corresponds to the initial drug content of ~ 10 mg of naproxen/HPβCD (1/1) IC nanofibrous film. The release behaviour of samples was also analyzed from the point of release kinetic by using different kinetic calculation models (see supporting information).

The dissolution profiles of naproxen (~0.7 mg) and nanofibrous films (~5 mg) of HPβCD, naproxen/HPβCD (1/1) IC and naproxen/HPβCD (1/2) IC was examined by placing each sample in a vial and then adding 5 ml PBS to each of the vials. The simultaneous video was recorded to follow the dissolution behaviour (Video S1). Here, the concentration of nanofibrous films (~ 1mg/mL) was kept same with *in vitro* release test. On the other hand, the evaluation of disintegration profile was carried out in a medium that emulated the oral cavity moist environment. For this, filter paper (Fisherbrand, P5 Grade, ⌀: 7 cm, medium porosity, cellulose) was located on the Petri dishes (⌀: 10 cm) and saturated with 10 mL of the artificial saliva solution.[10] Afterwards, excess amount of medium was removed from the Petri dishes and then nanofibrous films of HPβCD, naproxen/HPβCD (1/1) IC and naproxen/HPβCD (1/2) IC (~ 6 X 7 cm) were placed individually on the wetted filter papers. Video S2 was concurrently recorded to reveal the disintegration behaviour of samples in artificial saliva environment.

Statistical analyses

The statistical analyses were performed through Origin Lab (Origin, 2023, USA). The one-way or two-way of variance (ANOVA) were applied with 0.05 level of probability.

Results and discussion

Morphology of nanofibrous film

Fig. 2 displayed the photos of electrospinning solutions and ultimate HPβCD, naproxen/HPβCD (1/1) IC and naproxen/HPβCD (1/2) IC nanofibrous films electrospun from these solutions along with their representative SEM images. Here, the HPβCD system was obtained as a clear solution (Fig. 2a-i) while naproxen/HPβCD (1/1) IC system yielded turbid one that was an indicator of the uncomplexed crystal naproxen existence in the solution (Fig. 2b-i). On the other hand, a clear solution was observed for the naproxen/HPβCD (1/2) IC system (Fig. 2c-i) just as in the HPβCD solution due to full complexation occurring between the drug and CD molecules in the aqueous solution. From all these three systems, free-standing, lightweight, and easily folded nanofibrous films were generated as a result of the electrospinning process as shown in Fig. 2a,b,c-i. The bead-free and uniform fiber formation for HPβCD, naproxen/HPβCD (1/1) IC and naproxen/HPβCD (1/2) IC nanofibrous films was demonstrated using SEM imaging (Fig. 2a,b,c-ii).

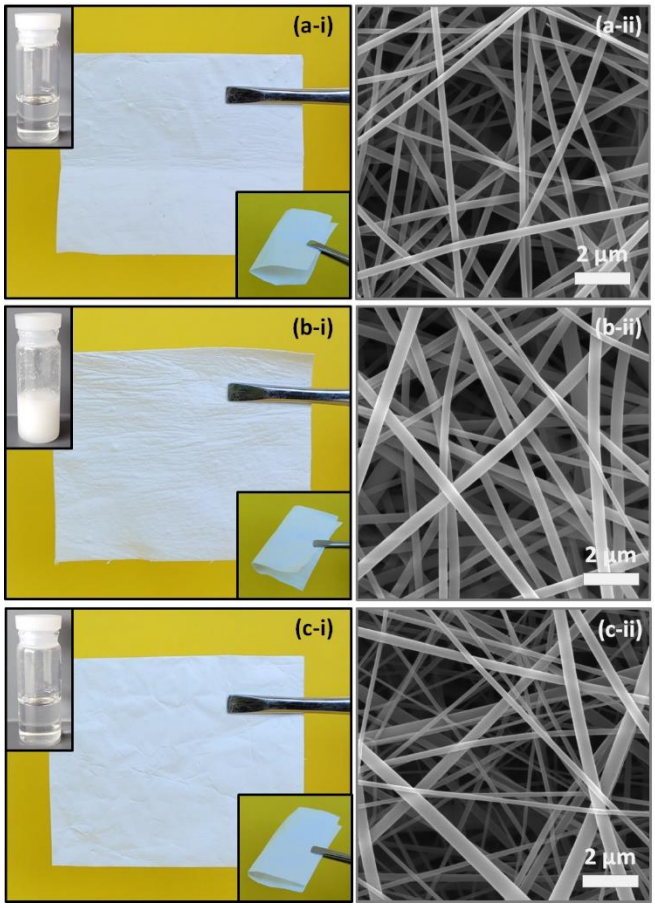

Fig. 2. (i) Photos of electrospinning solution and nanofibrous films and (ii) SEM images of nanofibrous films of (a) HPβCD, (b) naproxen/HPβCD (1/1) IC and (c) naproxen/HPβCD (1/2) IC.

The average fiber diameter (AFD) calculated from the SEM images and the solution properties including viscosity and conductivity were summarized in Table 1. As confirmed by the SEM images, thicker fibers were obtained for naproxen/HPβCD (1/1) IC nanofibrous film (260±70 nm) compared to naproxen/HPβCD (1/2) IC (180±90 nm) and HPβCD (195±45 nm) nanofibrous films (Table 1). The statistical analyses also depicted that the AFD of naproxen/HPβCD (1/1) IC nanofibrous film was significantly different from others ($p < 0.05$). Naproxen/HPβCD (1/1) IC system showed the highest viscosity (1.103 Pa·s) and lowest conductivity (40.95 µS/cm) among other two systems. This can be the explanation of thicker fiber formation than HPβCD and naproxen/HPβCD (1/2) IC nanofibrous films since less amount of electrical charge was formed in naproxen/HPβCD (1/1) IC solution and it led to less stretching during electrospinning (Table 1).[44]

Table 1. Solution properties and average fiber diameters (AFD, average ± std deviation) of electrospun nanofibers.

Sample	HPβCD conc. (%, w/w)[a]	Naproxen conc. (%, w/w)[b]	Viscosity (Pa·s)	Conductivity (µS/cm)	AFD (nm)
HPβCD	180	-	0.877	44.26	195±45
Naproxen/ HPβCD (1/1)	180	13.3	1.103	40.95	260±70
Naproxen/ HPβCD (1/2)	180	7.1	1.064	45.48	180±90

[a]with respect to solvent; [b]with respect to total sample amount

Structural characterization

FTIR analysis can offer an understanding of interactions between guest and CD molecules by inclusion complexation which can result in shifts or disappearances at the characteristic peaks of components.[45] Here, Fig. 3 depicted the full and expanded FTIR graphs of naproxen and nanofibrous films of HPβCD, naproxen/HPβCD (1/1) IC and naproxen/HPβCD (1/2) IC. The FTIR spectra of HPβCD nanofibrous film indicated characteristic bands belonging to HPβCD: 3350 cm^{-1} (stretching vibration of O–H), 2930 cm^{-1} (anti-symmetric vibration of CH_3), 1650 cm^{-1} (bending vibration of O–H), 1150 cm^{-1} (stretching vibration of C–O), 1023 cm^{-1} (stretching of antisymmetric C–O–C glycosidic bridge) (Fig. 3a).[46] The distinct characteristic peaks of HPβCD were also detected in the FTIR spectra of naproxen/HPβCD IC nanofibrous film due to higher portion of CD content in the film structure (~ 87-93 % (w/w)). For pure naproxen, the characteristic absorption peaks were observed at 1724-1682 cm^{-1} (–C=O stretching), 1602 cm^{-1} and 1505 cm^{-1} (C=C aromatic stretching), 1393 cm^{-1} (CH_3 bending), 1264 and 1027 cm^{-1} (symmetric aryl-O stretching), 1225 cm^{-1} (–O– stretching) (Fig. 3b,c).[30,31,39] All given characteristic peaks of naproxen were also observed in the FTIR graphs of naproxen/HPβCD (1/1) IC and naproxen/HPβCD (1/2) IC nanofibrous films and this proved the existence of naproxen molecules in these samples (Fig. 3b,c).

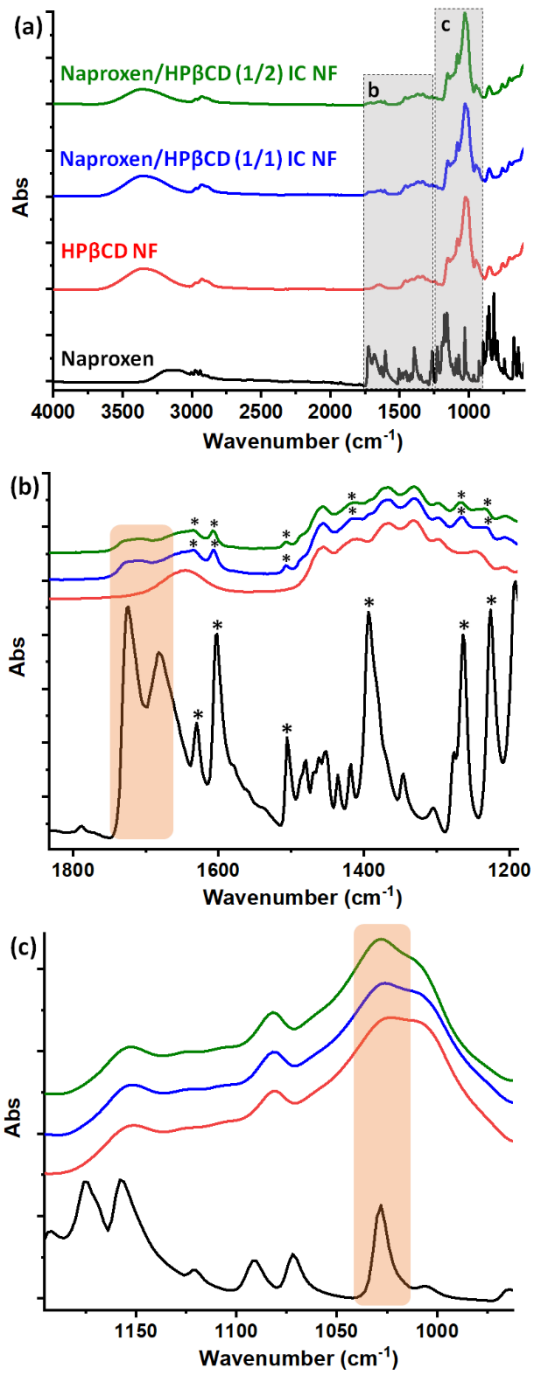

Fig. 3. (a) Full and (b,c) expanded FTIR graphs of naproxen, HPβCD NM, naproxen/HPβCD (1/1) IC NF and naproxen/HPβCD (1/2) IC NF (Nanofibrous film: NF).

Moreover, there was shift noticed for the characteristic peaks of naproxen in case of naproxen/HPβCD IC nanofibrous films from 1631 cm^{-1}, 1602 cm^{-1}, 1505 cm^{-1}, 1393 cm^{-1}, 1264 cm^{-1} and 1225 cm^{-1} to 1634 cm^{-1}, 1607 cm^{-1}, 1507 cm^{-1}, 1417 cm^{-1}, 1265 cm^{-1} and 1230 cm^{-1}, respectively (Fig. 3b). This confirmed the inclusion complex formation between naproxen and HPβCD in both electrospun nanofibrous films of naproxen/HPβCD IC.

In this study, XRD was utilized to examine the potential transition of naproxen crystals into the amorphous state as a result of the

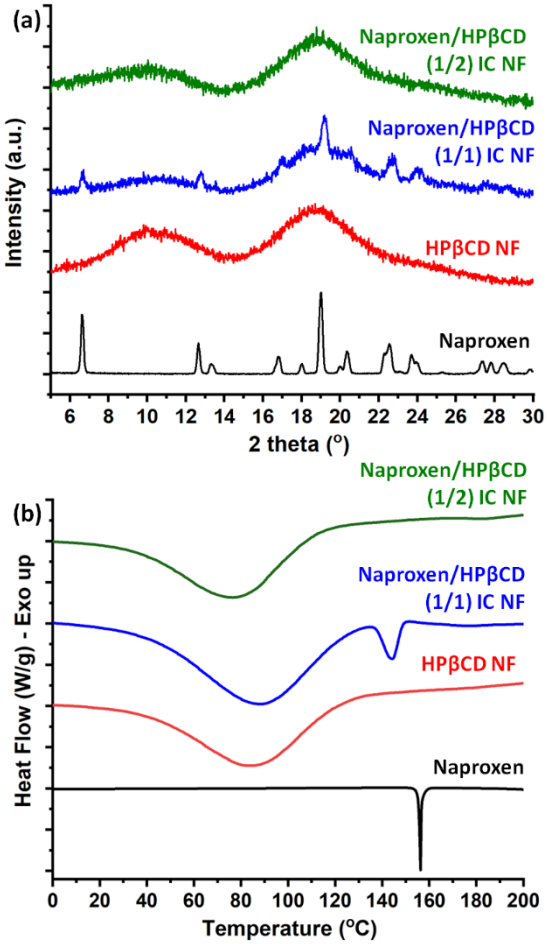

Fig. 4. (a) XRD (b) DSC graphs of naproxen, HPβCD NF, naproxen/HPβCD (1/1) IC NF and naproxen/HPβCD (1/2) IC NF (Nanofibrous film: NF).

inclusion complex formation with HPβCD. Fig. 4a showed the XRD graphs of naproxen and nanofibrous films of HPβCD, naproxen/HPβCD (1/1) IC and naproxen/HPβCD (1/2) IC. The distinct characteristic peaks of naproxen at 6.5°, 12.6°, 16.8°, 19.0°, 20.4°, 22.5° and 23.7° exhibited the crystalline nature of this drug.[47] On the other hand, broad halos (10° and 18.5°) were detected in case of HPβCD nanofibrous film owing to its amorphous state. For naproxen/HPβCD (1/1) IC nanofibrous film, the characteristic peaks of naproxen were observed demonstrating the existence of uncomplexed crystal drug parts within the sample. In contrast, the naproxen/HPβCD (1/2) IC nanofibrous film displayed an amorphous pattern identical to pristine HPβCD nanofibrous film as a result of complete complexation between naproxen and HPβCD which ensured the full amorphization drug crystals within the film.

The amorphous distribution of naproxen in naproxen/HPβCD (1/2) IC nanofibrous film and the presence of drug crystals in naproxen/HPβCD (1/1) IC nanofibrous film were further verified using DSC technique. Fig. 4b indicated the DSC thermograms of naproxen and nanofibrous films of HPβCD, naproxen/HPβCD (1/1) IC and naproxen/HPβCD (1/2) IC. Here, the DSC thermogram of naproxen showed endothermic peak at ~156°C corresponding the melting of drug crystals.[47] On the other hand, both HPβCD and

naproxen/HPβCD (1/2) IC nanofibrous film exhibited a broad endothermic peak at ~90 °C originating from dehydration of water content in samples. The melting peak of naproxen was detected at around 144°C with a broader feature compared to pure naproxen in the case of naproxen/HPβCD (1/1) IC nanofibrous film, and this is evidence for the existence of both complexed and uncomplexed naproxen within 1/1 based nanofibrous film.[45] Nonetheless, there was no distinct endothermic peak detected at the respective region of the thermogram for naproxen/HPβCD (1/2) IC nanofibrous film supporting the complete complexation between naproxen and HPβCD (Fig. 4b). It is obvious that the results of DSC aligned with both XRD findings (Fig 4a) and visual observations of solution photos (Fig. 2).

Here, TGA technique was applied to investigate the thermal degradation profile of nanofibrous films. Fig. 5 displayed the TGA thermograms and derivative thermograms (DTG) of naproxen and nanofibrous films of HPβCD, naproxen/HPβCD (1/1) IC and naproxen/HPβCD (1/2) IC. For nanofibrous films, the weight-loss step completed at around 100 °C corresponded the water dehydration from the samples. On the other hand, the main weight-loss observed at ~ 360°C was due to thermal degradation of HPβCD within the nanofibrous films (Fig. 5a). Differently from pristine HPβCD nanofibrous film, an additional step was observed at ~305°C in the case of naproxen/HPβCD IC ones which raised from the naproxen content (Fig. 5b). However, it is obvious that the thermal degradation of naproxen occurred at higher temperature for naproxen/HPβCD IC nanofibrous film when compared to pure naproxen degradation that happened at around 255°C (Fig. 5b).[33] This shift also confirmed the inclusion complex formation between naproxen and HPβCD which required higher level of energy for the thermal degradation process. TGA analysis can also provide information about the approximate content (%) of components within the samples. Here, the TGA thermograms of naproxen/HPβCD IC nanofibrous film did not allow this calculation since the thermal degradation of naproxen overlapped with the main degradation of HPβCD. Even so, the DTG graphs clearly exhibited the differences in naproxen and HPβCD contents between naproxen/HPβCD (1/1) IC and naproxen/HPβCD (1/2) IC nanofibrous films. Such that, the step intensity of naproxen was found to be lower in the case of naproxen/HPβCD (1/2) IC nanofibrous film compared to naproxen/HPβCD (1/1) IC one while it was higher for HPβCD weight-loss step. This finding supported the lower drug content of naproxen/HPβCD (1/2) IC nanofibrous films (~ 7.1 %, w/w) than naproxen/HPβCD (1/1) IC nanofibrous films (~ 13.3 %, w/w).

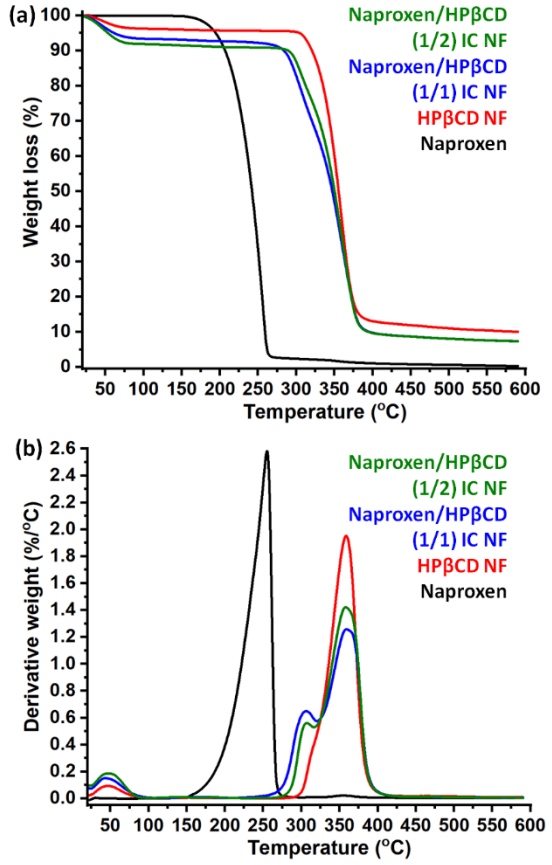

Fig. 5. (a) TGA thermograms and (b) derivative thermograms (DTG) of naproxen, HPβCD NF, naproxen/HPβCD (1/1) IC NF and naproxen/HPβCD (1/2) IC NF (Nanofibrous film: NF).

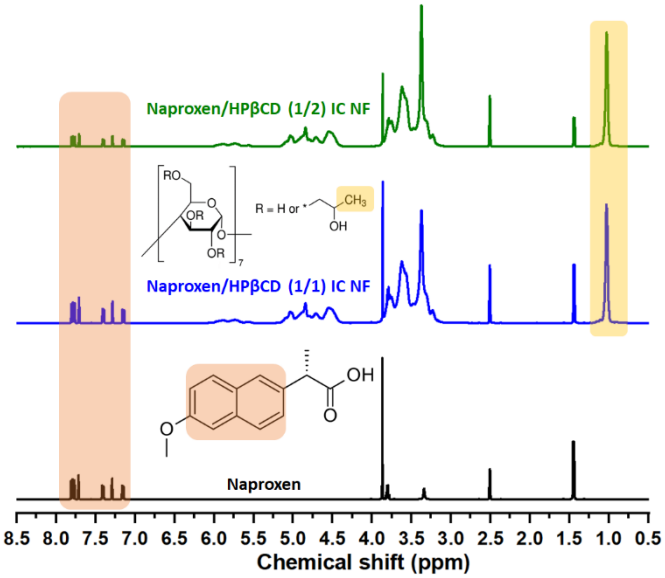

Fig. 6. ^{1}H-NMR spectra of naproxen, naproxen/HPβCD (1/1) IC NF and naproxen/HPβCD (1/2) IC NF (Nanofibrous film: NF).

Loading efficiency of nanofibrous films

The electrospinning solutions of naproxen/HPβCD IC systems were prepared using 1/1 and 1/2 molar ratios (drug/CD) that respectively corresponded to 13.3 % and 7.1 % (w/w) of naproxen content in the electrospun nanofibrous films. The loading efficiency test revealed that the ultimate nanofibrous films of naproxen/HPβCD (1/1) IC and naproxen/HPβCD (1/2) IC were respectively obtained with 83.73±4.36 % and 100.03±3.51 % (w/w) loading efficiency that corresponded to ~ 11.1 % and ~ 7.1 % (w/w) of naproxen content. The statistical analyses also demonstrated the significant difference between samples ($p < 0.05$). In other words, there was detected a slight loss of naproxen in the case of naproxen/HPβCD (1/1) IC nanofibrous film and this was most likely originated from the uncomplexed parts of drug molecules which caused heterogeneity in its electrospinning solution. On the other hand, no drug loss was noticed for naproxen/HPβCD (1/2) IC nanofibrous films owing to

complete complexation attained between naproxen and HPβCD within the sample.

Here, ^{1}H-NMR analysis was also performed to examine the chemical structure and rough content of naproxen molecules within nanofibrous films. Fig. 6 showed the ^{1}H-NMR spectra of naproxen and nanofibrous films of naproxen/HPβCD (1/1) IC and naproxen/HPβCD (1/2) IC. It was found that the characteristic peaks of naproxen represented the same pattern in the ^{1}H-NMR spectra of naproxen/HPβCD (1/1) IC and naproxen/HPβCD (1/2) IC nanofibrous films. This demonstrated the preserved chemical structure of this drug molecule during the whole process. On the other hand, the highlighted parts signified the non-overlapped integrated peaks of naproxen and HPβCD were used to calculate the molar ratio of the ultimate nanofibrous films (Fig. 6). For naproxen, the peaks located between 7 ppm to 8 ppm and corresponded to the aromatic ring of the molecule were taken into account during the calculation.[39] For HPβCD, the peak located at ~ 1 ppm and corresponded to methyl group was used for the analysis.[20] The results revealed that the molar ratio (drug/CD) was found to be 1.00/1.04 and 1.00/1.97 for naproxen/HPβCD (1/1) IC and naproxen/HPβCD (1/2) IC nanofibrous films, respectively which corresponding ~96.1 % and ~101.5 % (w/w) loading efficiency. These findings are approximately the same as the results of the loading efficiency test however, the difference distinguished for naproxen/HPβCD (1/1) IC nanofibrous film might be due to the variations between test techniques. Briefly, naproxen was effectively encapsulated into nanofibrous films with different loading contents (~7-11%, w/w) due to inclusion complexation between drug and CD molecules.

2D-NMR (ROESY) analysis

ROESY technique enables to probe interactions over extended distances up to 5 Å, so it is distinguished for the investigation of nanoscale assemblies constructed with CD.[48] Therefore, 2D-NMR (ROESY) measurement was also performed to examine the spatial interactions within the inclusion complexes of naproxen and HPβCD. Fig. 7 depicts the existence of spatial interaction between the H atoms of host and guest molecules by the cross-peaks. The expanded ROESY spectra (Fig. 7b) was the evident of concurrent proton resonances between the inner cavity protons (H_3 and H_5) of the HPβCD and the aromatic protons of naproxen. In other words, the ROESY finding further revealed that the aromatic part of naproxen was encapsulated in the hydrophobic cavity of HPβCD by inclusion complexation.

Computational analysis

The interaction between naproxen and HPβCD, and the formation of IC were examined by first-principles computational methods. First, the ground state configurations of naproxen and HPβCD were obtained individually by relaxing structures in a vacuum. Next, the interaction between them was analyzed by varying the position and orientation of naproxen. The gradual decrease in total energy as naproxen approaches HPβCD indicated that interaction was energetically favourable and providing activation energy was not required for binding. While IC can be formed for tail (T) and head (H) horizontal orientations of naproxen, vertical arrangements did not fit due to size match. The ground state configurations for 1:1

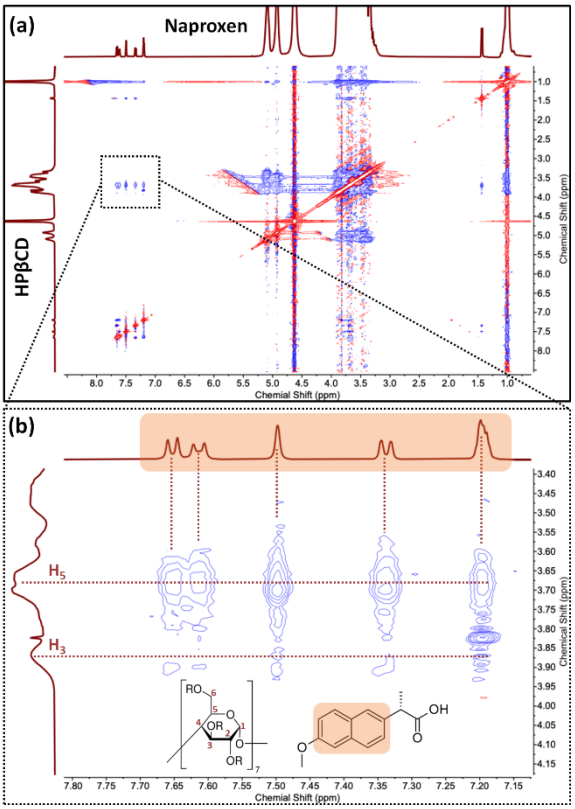

Fig. 7. (a) Full and (b) expanded 2D-NMR (ROESY) spectra of naproxen and HPβCD recorded in D_2O.

stoichiometry, where the total energy was minimum, and the force acting on the system was practically zero (below 0.01 eV/Å, which was set as a threshold value), were shown in Fig. 8a-b. At this point, complexation energy, which can be used to quantify the interaction strength, can be calculated as;

$$E_{CE} = n*E_T[\text{HP}\beta\text{CD}] + E_T[\text{naproxen}] - E_T[\text{naproxen/HP}\beta\text{CD IC}] \quad \text{(Formula 3)}$$

where E_T[HPβCD], E_T[naproxen], and E_T[naproxen/HPβCD IC] are the total energies (calculated in vacuum or solvent) of HPβCD, naproxen, and naproxen/HPβCD IC, respectively. *n* indicated the number of HPβCD in IC, which was 1 for 1:1 and 2 for 1:2 stoichiometry. The computed values were listed in Table 2. Positive values of E_{CE} point out the stability of the complex, and T-orientation through wide-rim (B) was energetically the most favourable configuration for 1:1 stoichiometry. Similarly, 1:2 stoichiometry was also examined, and four stable designs were shown in Fig. 8c-f. The obtained E_{CE} values were significantly larger than 1:1, implying that 1:2 was the preferred stoichiometry for naproxen/HPβCD IC. It should also be noted that the penetration through narrow-rim (A) reduces E_{CE} due to the HP arms. As a next step, the computations were repeated in water to reveal the influence of solvent on the attained properties. While the effect of water on structures was found to be minute, a notable decrease in E_{CE} was recognized (Table 2). This decrease marked a reduction in the binding strength between naproxen and HPβCD. Once the total energies of the structures and IC were calculated, the solvation energy (E_{SE}) of the system can be estimated. E_{SE} is defined as;

$$E_{SE} = E_T^{Solv} - E_T^{Vac} \quad \text{(Formula 4)}$$

where E_T^{Solv} and E_T^{Vac} are the total energy of the IC in water and vacuum, respectively. As can be seen from Table 2, the E_{SE} of naproxen molecule increased from -9.5 kcal/mol up to -72.2 kcal/mol and -104.0 kcal/mol for 1:1 and 1:2 stoichiometries, respectively. The increase in $E_{SE,}$ in addition to a decrease in E_{CE} in water, signals an enhancement in solubility.

Table 2. The complexation and solvation energies of naproxen/HPβCD-IC for different orientations (Orient.) in 1:1 and 1:2 stoichiometry (drug:CD). T and H indicates tail and head orientations of naproxen; A and B indicates narrow and wide rims of HPβCD (See Fig. 8).

Drug:CD	Orient.	E_{CE}^{Vac} (kcal/mol)	E_{CE}^{Solv} (kcal/mol)	E_{SE} (kcal/mol)
1:1	B-H	6.25	-	-
	B-T	8.18	5.01	-72.16
1:2	B-HT-A	31.40	-	-
	B-HT-B	65.80	28.64	-104.04
	B-TH-A	24.38	-	-
	B-TH-B	66.84	29.34	-103.69

Pharmacotechnical profiles of nanofibrous films

The effect of increasing HPβCD concentrations against naproxen solubility was examined by phase solubility test (Fig. 9a). The intrinsic solubility of naproxen in the absence of HPβCD molecule was ~0.4 mM and ~12.3 times higher solubility was attained for the highest HPβCD concentration of 32 mM by inclusion complexation. From the linear part of phase solubility diagram, the binding constant (K_S) between naproxen and HPβCD was also calculated as 588 M^{-1}. As is shown in Figure S1, the pH of the phase solubility test solutions decreased from 5.6 to 4.1 as the HPβCD concentration increased from 0 to 32 mM. Here, the decline observed at the pH values can be attributed to the increasing amount of solubilized naproxen in the aqueous systems by inclusion complexation since naproxen is a weak acid compound with pKa 4.2 value.[49] The other related reports in which the inclusion complexes of naproxen and HPβCD were studied, revealed different K_S values. For instance, K_S values were reported as 2080 M^{-1} and 2083 M^{-1} for unbuffered systems of which pH was recorded at around 4.5[35] and 5[37], respectively. On the other hand, 1123 M^{-1} and 624 M^{-1} were observed for buffer-based systems respectively having pH 7[30] and 1.[50] In another related study of Cirri et al., K_S values were found to be 4890 M^{-1}, 2605 M^{-1} and 230 M^{-1} for the buffered systems with 1.1, 4.0 and 6.5 pH values, respectively.[49] Here, K_S of the naproxen/HPβCD couple decreased as the pH value increased and this was assigned to the progressive rise of the naproxen ionized form that shows a lower affinity for the apolar hydrophobic cavity of HPβCD.[49] However, it is still obvious that different K_S values can be obtained from the phase solubility analysis of the same host-guest (CD:drug) system. These variations can be ascribed to differences in the purity degree of molecules, CD concentration ranges used in the experiments, and/or substitution degree of HPβCD.[49,51,52]

In this study, the time dependent release of naproxen from naproxen/HPβCD (1/1) IC and naproxen/HPβCD (1/2) IC nanofibrous films were examined in PBS buffer system having pH 7.4. Fig. 9b

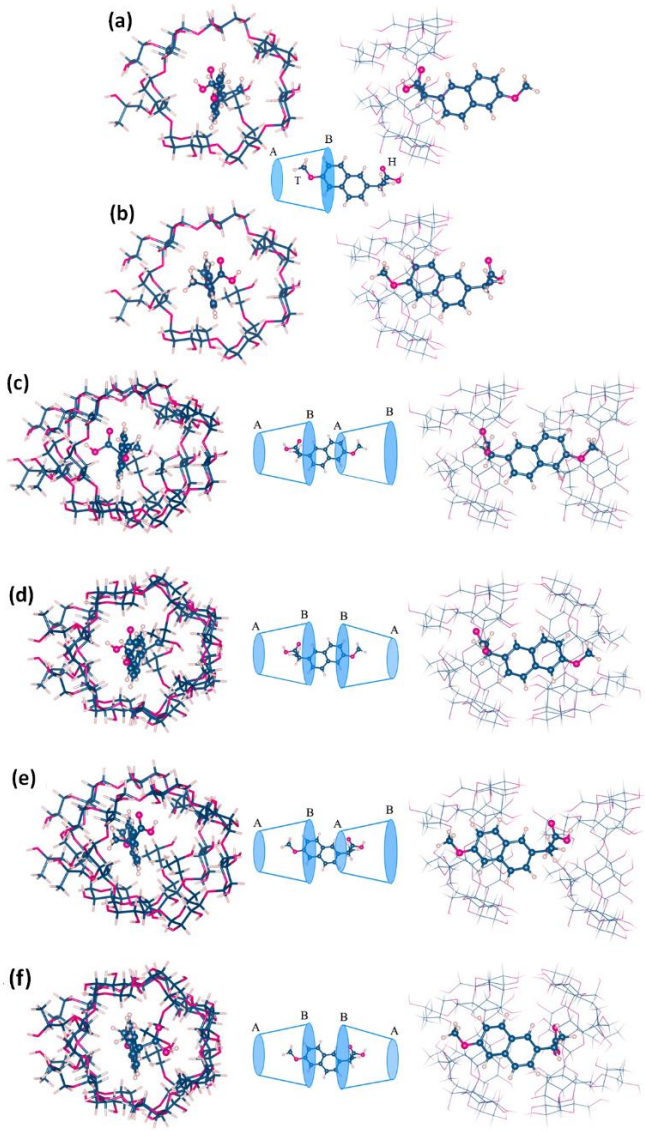

Fig. 8. The top and side views of naproxen/HPβCD IC in (a) B-T and (b) B-H orientations for 1:1 stoichiometry; (c) B-HT-A (d) B-HT-B (e) B-TH-A (f) B-TH-B orientations for 1:2 stoichiometry.

indicates the release graphs of nanofibrous films comparatively with pure naproxen. As is seen, naproxen/HPβCD (1/2) IC nanofibrous film reached the release concentration of 65.72±7.01 ppm in 30 seconds, showed almost plateau profile over 10 minutes, and completed this period with 69.44±5.82 ppm of naproxen release (Fig. 9b). Here, naproxen/HPβCD (1/1) IC nanofibrous film also showed a fast release behaviour by releasing 136.05± 4.12 ppm of naproxen in the first 30 seconds. Then, it reached to release concentration of 154.74±1.65 ppm till the end of 10 minutes with a slight increasing trend. On the other hand, pure naproxen displayed a release based on the dissolution of the drug in PBS buffer with a concentration of 7.24±1.94 ppm in the first 30 seconds, and got the release of 19.14±2.76 ppm at the end of 10 minutes (Fig. 9b). The remarkable difference between samples were also established by the statistical analysis ($p<0.05$). The variation between released concentration of nanofibrous films were accordant with and proceeded from the naproxen content of naproxen/HPβCD (1/1) IC (~ 13 %, w/w) and

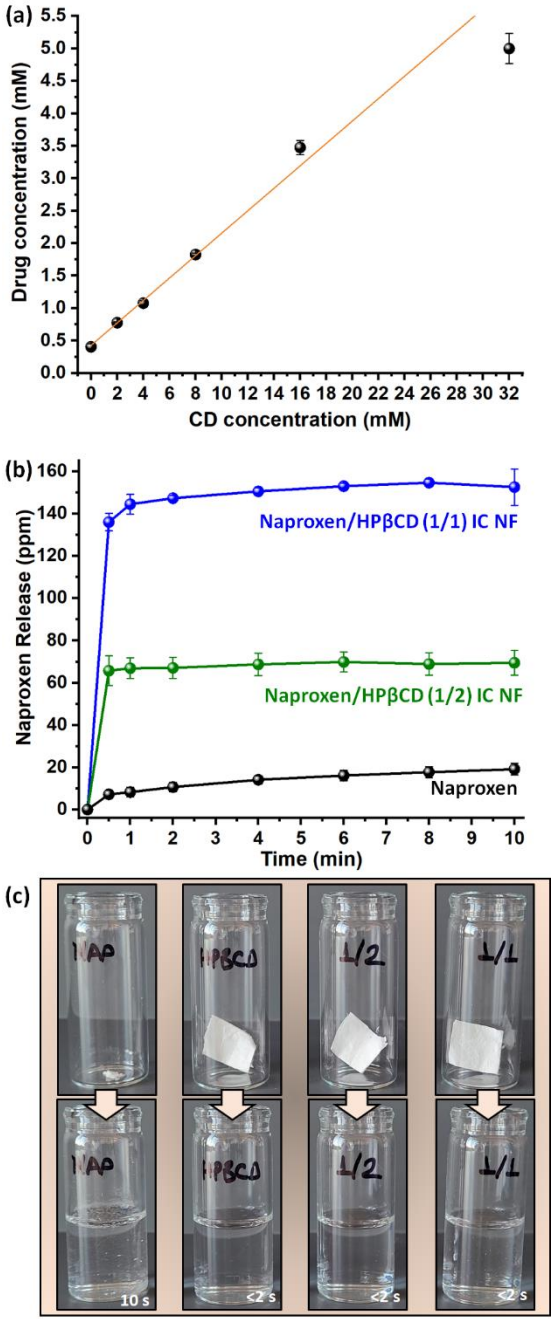

Fig. 9. (a) Phase solubility diagram of naproxen against increasing HPβCD concentrations. (b) *In vitro* time-dependent release profile of naproxen, naproxen/HPβCD (1/1) IC NF and naproxen/HPβCD (1/2) IC NF. (c) The dissolution profiles of (captured from Video S1) naproxen, HPβCD NF, naproxen/HPβCD (1/1) IC NF and naproxen/HPβCD (1/2) IC NF (Nanofibrous film: NF).

naproxen/HPβCD (1/2) IC (~ 7%, w/w) systems. For naproxen/HPβCD (1/1) IC nanofibrous films, the increment tendency detected on release amount of naproxen in the given time period might be due to time-dependent dissolution of drug crystals having an uncomplexed state existing in the samples. On the other hand, the inclusion complex formation between naproxen and HPβCD made possible to reach enhanced and faster release of naproxen from nanofibrous films compared to pure naproxen owing to amorphous state and so improved water solubility of naproxen in the nanofibrous films. The notable aqueous solubility of HPβCD (> 2000 mg/mL) can be also considered one of the main reasons to attain this better release profile in the case of nanofibrous films by their fast dissolution in the PBS medium. The dissolution profile of samples was followed visually as shown in Fig. 9c and Video S1. Here, pure naproxen did not dissolve completely in PBS buffer due to its limited solubility, and undissolved particles remained floating in aqueous medium. In contrast, the nanofibrous films of HPβCD, naproxen/HPβCD (1/1) IC and naproxen/HPβCD (1/2) IC instantly dissolved with the contact of medium (Fig. 9c). While naproxen/HPβCD (1/2) IC nanofibrous film dissolved close to that of pure HPβCD nanofibrous film without remaining any particles, few undissolved particles of naproxen were detected in the solution of naproxen/HPβCD (1/1) IC nanofibrous film. This finding also reflected the whole amorphous state and incomplete inclusion complexation in the case of naproxen/HPβCD (1/2) IC and naproxen/HPβCD (1/1) IC nanofibrous films, respectively.

The release behaviour of samples was supplementary inspected by various kinetic models. The formulations and their results (R^2, regression coefficient) were given in supporting information (Table S1). The kinetic model calculations demonstrated that the release profile of nanofibrous films did not adapt with the applied models of zero/first-order, Higuchi and Hixson-Crowell models (Table S1). This showed that the release of naproxen was not coherent with Fick`s first law displaying the time-dependent release from an insoluble matrix.[53] However, comparatively better consistency was detected with Korsmeyer-Peppas model revealing the erosion and diffusion-controlled release of naproxen from naproxen/HPβCD IC nanofibrous films. The release of naproxen represented consistency with almost all applied kinetic models by proving the prepotency of the Fickian diffusion mechanism and the progressive disintegration as a function of time for the release behaviour of this drug

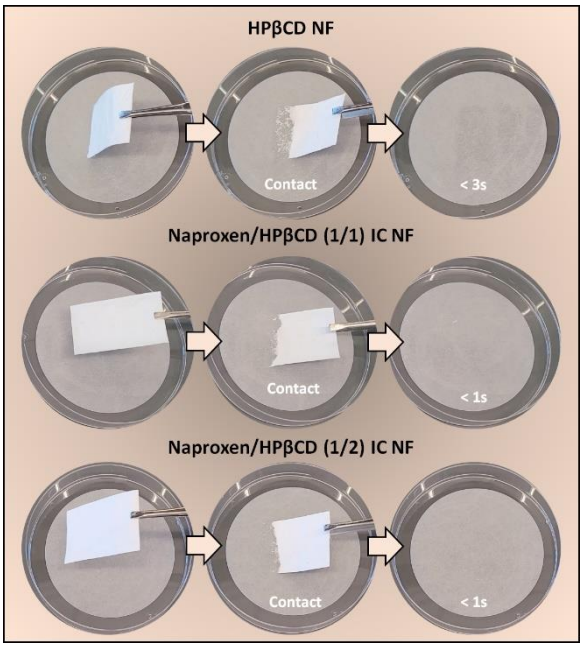

Fig. 10. Disintegration profiles of HPβCD NM, naproxen/HPβCD (1/1) IC NF and naproxen/HPβCD (1/2) IC NF (captured from Video S2) (Nanofibrous film: NF).

molecule.[53,54] Korsmeyer-Peppas equation also enabled the calculation of the diffusion exponent (*n*) value, and it was detected in the range of 0.45<n<0.89 for all samples pointing out the irregular diffusion of naproxen into the aqueous medium.[53]

For the examination of disintegration profile, the moist environment of oral cavity was simulated using a filter paper which were saturated with an artificial saliva medium.[10] Fig. 10 indicated the photos caught from Video S2. It is obvious that naproxen/HPβCD IC nanofibrous films were immediately absorbed by wetted filter paper in less than a second just after contact (Fig. 10). The impressive disintegration behaviour of nanofibrous films is essentially owing to unique properties including the highly water-soluble nature of HPβCD, and the high surface area and the high porosity of nanofibrous films which create additional access channels and active sides during the penetration of aqueous medium within fiber structures.[7] Consequently, naproxen/HPβCD IC nanofibrous films would be appropriate fast-disintegrating delivery systems for oral applications by ensuring rapid release and disintegration features and without giving an unfavourable granular sense during treatments. This approach can be carried one step further by conceiving nanofibrous films having multiple-phase releases with initial fast release profile.[55,56]

Conclusions

In this study, the polymer-free nanofibrous film of naproxen/HPβCD IC was generated with two different molar ratios of 1/1 and 1/2 (drug/CD) having uniform morphology with ~260 nm and ~180 nm of average fiber diameter, respectively. Naproxen/HPβCD IC nanofibrous films were obtained in water and in the absence of toxic chemicals. While full amorphous distribution of naproxen was provided in naproxen/HPβCD (1/2) IC nanofibrous film due to complete complexation, the uncomplexed naproxen parts were detected in the case of naproxen/HPβCD (1/1) IC nanofibrous film. Accordingly, naproxen/HPβCD (1/1) IC and naproxen/HPβCD (1/2) IC nanofibrous films were respectively attained with ~ 84% and ~100 % loading efficiency that corresponds to ~ 11% and ~7 % (w/w) drug content. The complexation energy calculated by the modeling study also demonstrated a more favourable interaction between HPβCD and naproxen for 1/2 molar ratio compared to 1/1 (drug/CD). Additionally, 2D-NMR (ROESY) results supported the complex formation between naproxen and HPβCD molecules by the encapsulation of the aromatic part of naproxen into the hydrophobic cavity of HPβCD. Here, highly porous structure, high surface area and extremely high-water solubility of HPβCD (> 2000 mg/mL) made possible the fast-dissolution of naproxen/HPβCD IC nanofibrous films in water. The amorphous state of naproxen raised from inclusion complexation within nanofibrous films ensured a faster release for naproxen than its pure crystal form. In addition, naproxen/HPβCD IC nanofibrous films disintegrated in the artificial saliva environment in less than a second. Briefly, the findings displayed that naproxen/HPβCD IC nanofibrous films can be a promising alternative dosage form for the treatment of naproxen as an orally fast-disintegrating drug delivery system. Further research on electrospun nanofibrous films of different drugs using CD inclusion complexes would be valuable for the progress and understanding of this fast-disintegrating systems.

Author Contributions

A. C. took part in conseptualization, methodology, investigation and writing-original draft. K. D. took part in the investigation and writing-original draft. M. A. took part in 2D-NMR and pH values investigation. M. E. K. and E. D. took part in investigation-computational modeling and writing-computational modeling. T. U. took part in conseptualization, methodology, editing, funding acquisition and project administration.

Conflicts of interest

There are no conflicts to declare.

Acknowledgements

This work made use of the Cornell Center for Materials Research Shared Facilities which are supported through the NSF MRSEC program (DMR-1719875), and the Cornell Chemistry NMR Facility supported in part by the NSF MRI program (CHE-1531632), and Department of Human Centered Design facilities. M.E.K acknowledges support from Brain Pool Program through the National Research Foundation of Korea (NRF) funded by the Ministry of Science and ICT (2020H1D3A1A02081517).

References

1 S. Kalepu and V. Nekkanti, *Acta Pharm. Sin. B*, 2015, **5**, 442–453.
2 F. Ditzinger, D. J. Price, A.-R. Ilie, N. J. Köhl, S. Jankovic, G. Tsakiridou, S. Aleandri, L. Kalantzi, R. Holm and A. Nair, *J. Pharm. Pharmacol.*, 2019, **71**, 464–482.
3 M. He, L. Zhu, N. Yang, H. Li and Q. Yang, *Int. J. Pharm.*, 2021, **604**, 120759.
4 E. Turković, I. Vasiljević, M. Drašković and J. Parojčić, *J. Drug Deliv. Sci. Technol.*, 2022, 103708.
5 J. Boateng, *J. Pharm. Sci.*, 2017, **106**, 3188–3198.
6 M. Almukainzi, G. L. B. Araujo and R. Löbenberg, *J. Pharm. Investig.*, 2019, **49**, 229–243.
7 D.-G. Yu, J.-J. Li, G. R. Williams and M. Zhao, *J. Control. release*, 2018, **292**, 91–110.
8 Y. Si, S. Shi and J. Hu, *Nano Today*, 2023, **48**, 101723.
9 S. M. Tan, X. Y. Teoh, J. Le Hwang, Z. P. Khong, R. Sejare, A. Q. A. Al Mashhadani, R. Abou Assi and S. Y. Chan, *J. Drug Deliv. Sci. Technol.*, 2022, 103761.
10 B. Balusamy, A. Celebioglu, A. Senthamizhan and T. Uyar, *J. Control. release*, 2020, **326**, 482–509.
11 H. Liu, Y. Dai, J. Li, P. Liu, W. Zhou, D.-G. Yu and R. Ge, *Front. Bioeng. Biotechnol.*, 2023, **11**, 1172133.
12 M. Wang, R.-L. Ge, F. Zhang, D.-G. Yu, Z.-P. Liu, X. Li, H. Shen and G. R. Williams, *Biomater. Adv.*, 2023, **150**, 213404.
13 H. Lv, Y. Liu, P. Zhao, Y. Bai, W. Cui, S. Shen, Y. Liu, Z. Wang and D.-G. Yu, *Appl. Catal. B Environ.*, 2023, **330**, 122623.
14 S. Nam, S. Y. Lee and H.-J. Cho, *J. Colloid Interface Sci.*, 2017, **508**, 112–120.
15 N. Sharifi, S. A. Mortazavi, S. Rabbani, M. Torshabi, R.

Talimi and A. Haeri, *J. Drug Deliv. Sci. Technol.*, 2022, 103356.
16 H. Bukhary, G. R. Williams and M. Orlu, *Int. J. Pharm.*, 2018, **549**, 446–455.
17 E. Hsiung, A. Celebioglu, R. Chowdhury, M. E. Kilic, E. Durgun, C. Altier and T. Uyar, *J. Colloid Interface Sci.*, 2022, **610**, 321–333.
18 E. Hsiung, A. Celebioglu, M. E. Kilic, E. Durgun and T. Uyar, *Mol. Pharm.*, 2023, **20**, 2624–2633.
19 M. Irfan, S. Rabel, Q. Bukhtar, M. I. Qadir, F. Jabeen and A. Khan, *Saudi Pharm. J.*, 2016, **24**, 537–546.
20 E. Hsiung, A. Celebioglu, M. E. Kilic, E. Durgun and T. Uyar, *Int. J. Pharm.*, 2022, **623**, 121921.
21 A. Celebioglu, N. Wang, M. E. Kilic, E. Durgun and T. Uyar, *Mol. Pharm.*, 2021, **18**, 4486–4500.
22 A. Celebioglu and T. Uyar, *Mater. Sci. Eng. C*, 2021, **118**, 111514.
23 S. Gao, W. Feng, H. Sun, L. Zong, X. Li, L. Zhao, F. Ye and Y. Fu, *J. Agric. Food Chem.*, 2022, **70**, 7911–7920.
24 S. Gao, J. Jiang, X. Li, F. Ye, Y. Fu and L. Zhao, *J. Agric. Food Chem.*, 2021, **69**, 5871–5881.
25 S. Gao, X. Li, G. Yang, W. Feng, L. Zong, L. Zhao, F. Ye and Y. Fu, *Ind. Crops Prod.*, 2022, **176**, 114300.
26 S. Patil, A. Celebioglu and T. Uyar, *J. Drug Deliv. Sci. Technol.*, 2023, **85**, 104584.
27 A. Celebioglu and T. Uyar, *RSC Med. Chem.*, 2020, **11**, 245–258.
28 P. Jansook, N. Ogawa and T. Loftsson, *Int. J. Pharm.*, 2018, **535**, 272–284.
29 S. S. Braga, *J. Drug Deliv. Sci. Technol.*, 2022, 103650.
30 S. Mohandoss, N. Ahmad, M. R. Khan and Y. R. Lee, *J. Mol. Liq.*, 2023, 122411.
31 A. Mani, P. Ramasamy, A. A. M. Prabhu and N. Rajendiran, *J. Mol. Struct.*, 2023, **1284**, 135301.
32 S. Pereva, T. Sarafska, V. Petrov, S. Angelova and T. Spassov, *J. Mol. Struct.*, 2021, **1235**, 130218.
33 P. Mura, G. P. Bettinetti, M. Cirri, F. Maestrelli, M. Sorrenti and L. Catenacci, *Eur. J. Pharm. Biopharm.*, 2005, **59**, 99–106.
34 A. C. Illapakurthy, C. M. Wyandt and S. P. Stodghill, *Eur. J. Pharm. Biopharm.*, 2005, **59**, 325–332.
35 P. Mura, F. Maestrelli and M. Cirri, *Int. J. Pharm.*, 2003, **260**, 293–302.
36 B.-J. Lee and J.-R. Lee, *Arch. Pharm. Res.*, 1995, **18**, 22–26.
37 F. Melani, G. P. Bettinetti, P. Mura and A. Manderioli, *J. Incl. Phenom. Mol. Recognit. Chem.*, 1995, **22**, 131–143.
38 M. Séon-Lutz, A.-C. Couffin, S. Vignoud, G. Schlatter and A. Hébraud, *Carbohydr. Polym.*, 2019, **207**, 276–287.
39 M. F. Canbolat, A. Celebioglu and T. Uyar, *Colloids Surf. B: Biointerfaces*, 2014, **115**, 15–21.
40 G. Kresse and J. Furthmüller, *Comput. Mater. Sci.*, 1996, **6**, 15–50.
41 G. Kresse and J. Furthmüller, *Phys. Rev. B*, 1996, **54**, 11169.
42 S. Grimme, *J. Comput. Chem.*, 2006, **27**, 1787–1799.
43 K. Mathew, R. Sundararaman, K. Letchworth-Weaver, T. A. Arias and R. G. Hennig, *J. Chem. Phys.*, 2014, **140**, 84106.
44 J. Xue, T. Wu, Y. Dai and Y. Xia, *Chem. Rev.*, 2019, **119**, 5298–5415.
45 G. Narayanan, R. Boy, B. S. Gupta and A. E. Tonelli, *Polym. Test.*, 2017, **62**, 402–439.
46 C. Yuan, B. Liu and H. Liu, *Carbohydr. Polym.*, 2015, **118**, 36–40.
47 B. Rojek, M. Gazda and A. Plenis, *Spectrochim. Acta Part A Mol. Biomol. Spectrosc.*, 2023, 123048.
48 M. Haouas, C. Falaise, N. Leclerc, S. Floquet and E. Cadot, *Dalt. Trans.*
49 M. Cirri, F. Maestrelli, G. Corti, S. Furlanetto and P. Mura, *J. Pharm. Biomed. Anal.*, 2006, **42**, 126–131.
50 J. Blanco, J. L. Vila-jato, F. Otero and S. Anguiano, *Drug Dev. Ind. Pharm.*, 1991, **17**, 943–957.
51 S. Anguiano-Igea, F. J. Otero-Espinar, J. L. Vila-Jato and J. Blanco-Méndez, *Eur. J. Pharm. Sci.*, 1997, **5**, 215–221.
52 T. Loftsson, H. Frikdriksdóttir, A. M. Sigurkdardóttir and H. Ueda, *Int. J. Pharm.*, 1994, **110**, 169–177.
53 N. A. Peppas and B. Narasimhan, *J. Control. release*, 2014, **190**, 75–81.
54 R. Gouda, H. Baishya and Z. Qing, *J. Dev. Drugs*, 2017, **6**, 1–8.
55 D.-G. Yu and J. Zhou, *J. Pharm. Sci.*, 2023, **112**, 2719–2723.
56 J. Zhou, P. Wang, D.-G. Yu and Y. Zhu, *Expert Opin. Drug Deliv.*, 2023, **20**, 621–640.